International Journal of Technology

http://ijtech.eng.ui.ac.id

Research Article

Unravelling How pH Sequence Shapes Green-Synthesized TiO_2 Nanoparticles for Dye-Sensitized Solar Cells

Fairuz Septiningrum[1], Rizka Fahirah[1], Akhmad Herman Yuwono[1.2.3*], Muhammad[1], Nofrijon Sofyan[1,2], Donanta Dhaneswara[1,2], Nelson Jap[1], Danang Pamungkas Priambodo[3]

[1]Department of Metallurgical and Materials Engineering, Faculty of Engineering, Universitas Indonesia, Depok 16424, Indonesia

[2]Advanced Materials Research Center (AMRC), Faculty of Engineering, Universitas Indonesia, Depok 16424, Indonesia

[3]Energy Transition Laboratory, Interdisciplinary Engineering Research Unit-Faculty of Engineering, Universitas Indonesia, Depok 16424, Indonesia

*Corresponding author: ahyuwono@eng.ui.ac.id; Tel.: +6281314099878

Abstract: In this study, the influence of pH adjustment sequence during green synthesis on the structural evolution of TiO_2 nanoparticles was investigated, specifically examining whether the solution pH was modified before or after the addition of titanium(IV) isopropoxide (TTIP). *Jatropha multifida* leaf extract was employed as a natural reducing, capping, and stabilizing agent owing to its rich bioactive compounds, which are capable of directing nanoparticle formation. Two synthesis pathways were systematically compared: pre-pH adjustment, where the extract pH (∼5) was adjusted to acidic or basic conditions prior to TTIP addition, and post-pH adjustment, where TTIP was first introduced into the extract, followed by pH modification. The pH values were varied at 3, 7, and 10. The results revealed that the crystallite size increased with increasing pH, and for the same pH value, the post-pH adjustment route consistently produced larger crystallites than the pre-pH adjustment route. Following synthesis, all as-prepared samples were utilized as photoanodes in DSSCs, and their photovoltaic performance was evaluated via current–voltage (I–V) measurements under simulated solar illumination. The pre-pH 3 sample achieved the highest PCE of 5.52%, attributed to its smaller crystallite size, which provides a higher surface area, greater dye loading, and improved charge transport. Thus, the pre-pH adjustment method is more suitable for producing TiO_2 for DSSC applications. This study demonstrates that the timing of pH adjustment controls TiO_2 nucleation and growth, shaping its final structure, and affecting DSSC performance. It provides a simple, green, and scalable way to tune TiO_2 for improved solar cell efficiency.

Keywords: Dye-sensitized solar cells (DSSCs); Green synthesis; Morphology; pH sequence control; TiO_2 nanoparticle

1. Introduction

The growing demand for sustainable energy has placed renewable energy technologies at the forefront of scientific and industrial development (Hassan et al., 2024). Among these, solar energy is one of the most promising sources due to its abundance, cleanliness, and wide availability (Kabir et al., 2018). DSSCs have emerged as a cost-effective and flexible alternative to conventional silicon photovoltaics, supported by their simple fabrication, low material usage, and strong performance under low-light conditions (Sasikumar et al., 2024; Saud et al., 2024; Devadiga et al., 2021). The photoanode material, which must offer high surface area for dye adsorption and efficiently facilitate electron injection and transport, is a key factor influencing DSSC performance (Sawal et al., 2023; Mohammadian-Sarcheshmeh et al., 2020; Karim et al.,

https://doi.org/10.14716/ijtech.v17i1.8206
Received June 2025; Revised November 2025; Accepted December 2025

2019; Fan et al., 2017). Titanium dioxide (TiO_2) nanoparticles remain the most widely used photoanode material because of their chemical stability, suitable energy band structure, abundant, and non-toxicity (Priyono et al., 2018; Shakeel-Ahmad et al., 2017; Sofyan et al., 2017). Nanomaterials are vital in solar energy technologies because their nanoscale size and high surface area enhance light absorption, while their tunable shape, size, and optical properties further optimize device performance and stability (Aftab et al., 2025).

Over the past several decades, a variety of synthetic methods have been developed to produce titanium dioxide (TiO_2) nanoparticles with controlled size, morphology, and crystallinity (Liu and Wang, 2019; Talebzadeh et al., 2019; Wang et al., 2014). Conventional approaches, such as the sol–gel process, hydrothermal treatment, and precipitation methods, often rely on high reaction temperatures, corrosive solvents, or expensive surfactants and templating agents. These requirements not only increase the synthesis's environmental footprint but also present challenges in terms of scalability and cost-effectiveness (Ahmed et al., 2022). Green synthesis has gained attention as a more sustainable alternative to address these limitations. This approach utilizes naturally derived extracts from plants, fungi, or algae, which are rich in bioactive compounds, including polyphenols, flavonoids, alkaloids, and saponins, that can function as reducing, stabilizing, and capping agents during nanoparticle formation (Sarip et al., 2022; Srikar et al., 2016; Virkutyte and Varma, 2011). This bio-mediated approach reduces the use of hazardous chemicals while offering improved control over the nucleation, growth, and physicochemical properties of the obtained TiO_2 nanoparticles (Behzad et al., 2021; Gnanasangeetha and Suresh, 2020).

Among the various plant sources explored for green synthesis, *Jatropha multifida* has shown considerable promise owing to its high content of bioactive phytochemicals, including alkaloids, terpenoids, and phenolic compounds. These naturally occurring molecules possess functional groups capable of chelating metal ions, modulating hydrolysis and condensation kinetics, and acting as capping agents that stabilize nanocrystal growth (Dah-Nouvlessounon et al., 2023). These interactions can influence the nucleation process and restrict uncontrolled particle growth, enabling the formation of TiO_2 nanostructures with improved size uniformity and dispersion (Goutam et al., 2018). Despite the growing interest in using botanical extracts for the green synthesis of TiO_2, the mechanistic aspects that govern the formation and final structure of the material remain poorly understood. The influence of specific process parameters, such as precursor concentration, reaction pH, and the sequence of reagent addition, has not been systematically studied, limiting our ability to optimize the physicochemical properties of the resulting nanomaterials (Mulay et al., 2024).

One of the key factors influencing the final formation of TiO_2 nanoparticles is the pH of the reaction solution, which plays a critical role in controlling the hydrolysis and condensation behavior of titanium alkoxide precursors such as titanium(IV) isopropoxide (TTIP) (Tryba et al., 2016). In conventional synthesis protocols, the pH of the reaction solution is typically adjusted after the addition of the metal precursor (post-pH adjustment), as demonstrated by Sridevi et al., 2020. In their work, TiO_2 nanoparticles were synthesized via a sol–gel method under controlled pH conditions (pH 6, 8, and 10) to investigate the influence of pH on particle formation. The results showed that pH significantly affected the nucleation and growth of the TiO_2 particles. X-ray diffraction (XRD) analysis confirmed that all samples predominantly exhibited the anatase phase with minor brookite content. Transmission electron microscopy (TEM) revealed that the nanoparticles possessed a nearly spherical morphology, with average particle sizes varying as a function of pH. Specifically, the sample synthesized at pH6 yielded the smallest average particle size of approximately 7 nm, while those synthesized at pH8 and pH10 exhibited larger particle sizes of approximately 13.7 nm and 17.8 nm, respectively. This trend indicates that lower pH conditions favor the formation of smaller and more uniform TiO_2 nanoparticles due to faster hydrolysis and more controlled condensation rates of the Ti precursor.

In contrast to conventional sol–gel methods, several studies on green synthesis approaches have shown that increasing the pH of the reaction can reduce particle size. As reported by

Muniandy et al., 2017, the reaction pH significantly influenced the physicochemical properties of TiO_2 nanoparticles synthesized without organic solvents using TTIP and starch as a biotemplate. Higher pH conditions enhanced hydrolysis and stabilized the titania network, resulting in smaller, well-dispersed nanoparticles with a crystallite size of 8.9nm, compared to larger aggregates formed under acidic conditions with a crystallite size of 12.2 nm. A similar result was reported in the study by Hanafy et al., 2020. Titanium tetrachloride ($TiCl_4$) was used as the precursor, and aloe vera extract was used as a natural reducing and stabilizing agent. The synthesis was carried out under varying pH conditions (acidic, neutral, and basic) without the use of toxic solvents or high-temperature treatments. XRD analysis revealed that acidic conditions led to the formation of mixed anatase, rutile, and brookite phases, whereas neutral pH produced anatase and rutile, and basic pH resulted in pure anatase. High-resolution transmission electron microscopy (HRTEM) showed that the average particle size decreased with increasing pH: approximately 22.9, 15.8, and 13.3 nm at acidic, neutral, and basic pH, respectively. This trend indicates that higher pH promotes enhanced hydrolysis and nucleation control, resulting in the formation of smaller and more uniform TiO_2 nanoparticles.

Although the effects of pH on nanoparticle size, crystallinity, and phase composition are well documented, the timing of pH adjustment relative to precursor addition remains largely unexplored, particularly in green synthesis, where it may significantly alter the final product. In plant-mediated syntheses, where biomolecules influence precursor coordination and hydrolysis, adjusting pH before or after the addition of metal precursors may significantly affect nanoparticle formation. This study addresses this gap by investigating the impact of pH adjustment sequence on the green synthesis of TiO_2 nanoparticles using *Jatropha multifida* leaf extract, with emphasis on their application as photoanode materials in DSSCs. Two synthesis pathways were investigated: (1) pre-pH adjustment, in which the initial pH of the *J. multifida* leaf extract was adjusted prior to TTIP addition and (2) post-pH adjustment, in which TTIP was first introduced into the extract followed by pH elevation. The synthesized TiO_2 nanoparticles were characterized by Fourier transform infrared spectroscopy (FTIR), X-ray diffraction (XRD), and scanning electron microscopy (SEM) to evaluate their chemical, structural, and morphological properties. In addition, their photovoltaic performance was assessed in DSSC devices. This work provides insight into the role of reaction sequence in green synthesis, offering a simple and sustainable approach to tailor nanomaterials for solar energy applications.

2. Methods

2.1 Chemicals and materials used

J. multifida leaves were collected from Cijantung, an area in East Jakarta. Ethanol, sodium hydroxide (NaOH), hydrochloric acid (HCl), and acetic acid were purchased from Sigma-Aldrich (Darmstadt, Germany). Titanium(IV) isopropoxide (TTIP) was obtained from Sigma-Aldrich (India), while acetylacetone was sourced from Sigma-Aldrich (China). Triton X-100 and PVP were procured from Sigma-Aldrich (St. Louis, USA). The dye cis-diisothiocyanato-bis(2,2′-bipyridyl-4,4′-dicarboxylato)ruthenium(II) bis(tetrabutylammonium) (N719), platinum paste (Platisol T/SP), iodide/tri-iodide electrolyte (Iodolyte HI-30), and sealing polymer film (Meltonix) were obtained from Solaronix (Aubonne, Switzerland). All chemicals were used without further purification or treatment.

2.2 Extraction of *J. multifida* leaves

The leaves of *J. multifida* were separated from the stems, washed with tap water, and soaked in warm distilled (DI) water to remove dirt and bacteria. The cleaned leaves were dried in an oven to reduce their moisture content. Once dried, they were ground into a fine powder using a chopper. *J. multifida* leaf powder (15 g) was weighed and transferred into a glass beaker containing 100 ml of ethanol. The mixture was stirred and heated at 60℃ for 1 h. The extract solution was filtered through Whatmann No. 40 filter paper from Cytiva (China). The obtained

filtrate was stored and ready to be used for the next process.

2.3 Green synthesis of TiO_2 NPs

The green synthesis of TiO_2 in this study followed the method reported by Qamar et al., 2024 with some modifications. Green-synthesized TiO_2 nanoparticles were prepared using titanium(IV) isopropoxide (TTIP) as the titanium precursor. Sodium hydroxide (NaOH) and hydrochloric acid (HCl) was used as the pH-adjusting agents. In the pre-pH adjustment process, the pH of 50 mL *J. multifida* leaf extract (15% v/v) was adjusted before the dropwise addition of 6 mL of TTIP. During the post-pH adjustment process, TTIP was added dropwise to the extract before the reaction solution was adjusted to the desired pH. In both routes, the initial pH of the extract was approximately 5 and was modified to an acidic condition (pH 3) using HCl or to basic conditions (pH 7 and 10) using NaOH. After the precursor was completely added, the mixture was stirred at 50℃ for 3 h to allow the reaction to proceed. The solution was cooled to room temperature and centrifuged for ±15 min to separate the solid precipitate from the supernatant. The resulting precipitate was oven-dried and subsequently calcined at 500℃ for 2 h to improve the crystallinity and structural stability of the TiO_2 nanoparticles. The initial pH, pre-pH, and post-pH adjustment samples were denoted as Initial pH 5, Pre pH, and Post pH, respectively. Figure 1 illustrates the overall synthesis route.

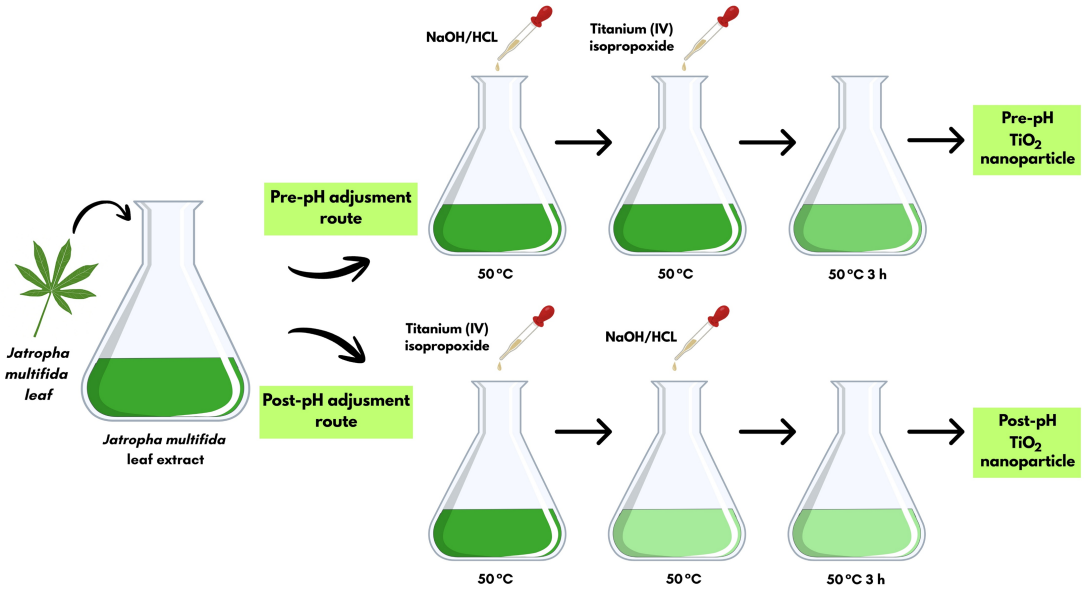

Figure 1 Schematic illustration of the synthesis procedures for TiO_2 samples prepared via pre-pH and post-pH adjustment routes

2.4 Fabrication of the DSSCs

To prepare the TiO_2 paste, 100 mg of the as-synthesized TiO_2 powder was mixed with 3 mL of ethanol, 0.1 mL of acetic acid, 0.04 mL of acetylacetone, 0.01 mL of Triton X-100, and 0.01 gr of PVP. The mixture was subsequently ground manually using an agate mortar and pestle for approximately 30min to obtain a uniform and homogeneous dispersion. Fluorine-doped tin oxide glass substrates (25 x 25 x 2.2 mm, 6Ω/cm^2) were masked with adhesive tape to define an active area of 0.25 cm^2. The TiO_2 paste was deposited via the doctor blade technique, annealed on a hot plate at 450℃ for 30 min, and then cooled to room temperature. A dye solution was prepared by dissolving 50 mi of cis-diisothiocyanato-bis(2,2′-bipyridyl-4,4′-dicarboxylato)ruthenium(II) bis(tetrabutylammonium) or N719 in 50 mL of ethanol. The dried TiO_2 photoanodes were immersed in the dye solution and kept in a sealed dark container overnight to ensure complete dye adsorption. Counter electrodes were prepared by drilling a 1-mm hole near the edge of the

FTO glass for electrolyte injection. Platinum paste was applied using the doctor blade method. After tape removal and cleaning, the counter electrodes were calcined at 450℃ for 30 min and cooled to room temperature. The device was assembled by sandwiching the photoanode and counter electrode with their conductive sides facing inward. A polymer-based spacer was inserted between the electrodes to prevent short-circuiting and was thermally sealed using a heat gun for 40 s. To avoid air entrapment, an iodide-based liquid electrolyte was injected through the predrilled hole using a syringe until the active area was fully infiltrated.

2.5 Characterizations

The infrared spectra of *J. multifida* leaf extract and the green-synthesized TiO_2 sample were obtained using FTIR (Fourier-transform infrared spectroscopy (FTIR, Shimadzu IRXross) over the wavenumber of 4000–400 cm-1. The phase structure of the as-prepared samples was analyzed using X-ray diffraction (XRD, Malvern PANalytical Empyrean) with a Cu Kα radiation source, scanned over a 2θ range of 20°–9020–90°, and the average crystallite sizes of the as-synthesized samples were calculated using Scherrer's equation (Uvarov and Popov, 2007):

$$d = \frac{K \times \lambda}{\beta \times \cos\theta} \tag{1}$$

where d is the crystallite size, λ is the X-ray wavelength, β is the full width at half maximum (FWHM), θ is the Bragg angle, and K is the Scherrer constant. The surface morphology was examined using field-emission scanning electron microscopy (FESEM, JEOL JSM-IT710HR LA). The photovoltaic performance of the DSSCs was evaluated by measuring the J–V characteristics under AM 1.5 illumination (100 mW cm^{-2}) using a solar simulator (Newport Sol 3A).

3. Results and Discussion

To identify the biomolecules responsible for the reduction and stabilization of nanoparticles, the FTIR spectrum of J. multifida leaf extract was compared with those of green-synthesized TiO_2 nanoparticles (initial-pH 5) and commercial TiO_2 (P25, Degussa GmbH, Germany) at wavenumber 4000 to 400 cm-1, as shown in Figure 2a. The FTIR spectrum of the *J. multifida* leaf extract shows a broad peak at 3319.44 cm^{-1} corresponding to O-H stretching, indicating phenolic compounds. The minor peaks at 2947.18 and 2829.26 cm^{-1} are associated with C–H stretching (Lee et al., 2019). Peaks appearing at approximately 1400 and 1000 cm^{-1} correspond to C=C bonding and C-O bonding or alcohol-related vibrations, respectively (Sofyan, Muhammad, et al., 2025). An additional O–H absorption band appears at 615.75 cm−1 (Saini and Kumar, 2023). The FTIR spectrum of green TiO_2 closely resembles that of commercial TiO_2, confirming the successful synthesis of TiO_2 nanoparticles via a green route, which is there is Ti-O-Ti stretching mode, indicating the bonding between Ti and oxygen (Nethravathi et al., 2021).

As shown in Figure 2b, all the as-synthesized samples exhibited similar FTIR patterns. A weak broad O–H stretching band appears between 3000–3500 cm^{-1}, while a weak band at 2340 cm^{-1} may arise from O–C–O vibrations introduced during green synthesis (Sofyan, Muhammad, et al., 2025). The absorption near 1500 cm^{-1} corresponds to C=C stretching, indicating the presence of aromatic compounds (Golthi et al., 2024). The Ti–O–Ti stretching mode also appears around 600 cm^{-1}, consistent with previous reports of biogenic TiO_2 (Sofyan, Rilda, and and, 2025; Thammaacheep et al., 2024). Moreover, in green TiO_2 synthesis, these functional groups act not only as reductors but also as stabilizers that enhance the surface reactivity of nanoparticles (Sangeetha et al., 2024; Singh et al., 2022).

Additionally, the use of ethanol as the extraction solvent promotes a higher yield of polyphenolic compounds with strong reducing capability. This is consistent with previous studies reporting that *J. multifida* leaf extract contains up to 23.03 ± 6.9 mg EqGA/g of polyphenols in ethanol-based extractions, thereby improving the efficiency of TiO_2 nanoparticle formation (Dah-Nouvlessounon et al., 2023).

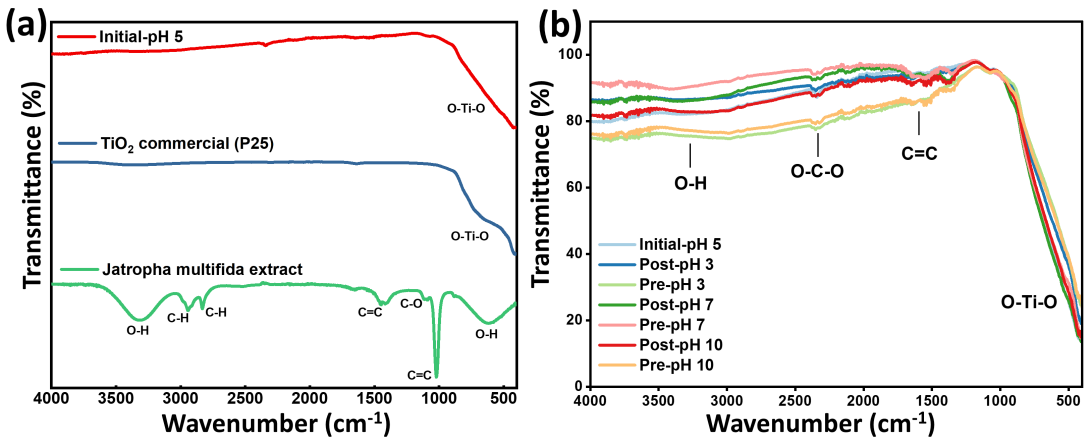

Figure 2 FTIR spectra of *Jatropha multifida* leaf extract, commercial TiO_2 (P25), green-synthesized TiO_2 (initial-pH 5) (a), and all the as-prepared samples (b)

In this study, we investigated the effect of pH adjustment sequence on the structural and morphological properties of green-synthesized TiO_2 nanoparticles, aiming to identify the optimal characteristics for their application as photoanode materials in DSSCs. The initial pH of the reaction mixture was approximately 5 and subsequently adjusted to pH 3 using hydrochloric acid (HCl) and to pH 7 and 10 using sodium hydroxide (NaOH). Figure 3 shows the X-ray diffraction (XRD) analysis of both synthesis routes, post-pH adjustment, and pre-pH adjustment. All samples exhibited distinct diffraction peaks corresponding to the tetragonal anatase phase of TiO_2, which was consistent with the reference pattern ICDS No. 01-071-1168. The observed peaks at 2θ values around 25.18°, 37.50°, 47.83°, 53.58°, 54.82°, 62.33°, and 68.28°are indexed to the (101), (004), (200), (105), (211), (204), and (116) crystal planes, respectively.

The average crystallite sizes calculated using Equation (1) are summarized in Table 1. Commercial TiO_2 (P25) was used as a reference and exhibited an average crystallite size of 22.95 nm. The initial sample (Initial-pH 5) synthesized via the green synthesis method had an average crystallite size of 24.02 nm. In the pre-pH adjustment route, the crystallite size decreased at lower pH but slightly increased with increasing pH, resulting in crystallite sizes of 16.38, 15.62, and 17.65 nm at pH 3, 7, and 10, respectively. Similarly, in the post-pH adjustment route, the crystallite size decreased from the initial condition but increased with higher pH, yielding 17.58, 18.50, and 19.24 nm at pH 3, 7, and 10, respectively. These results indicate that the post-pH adjustment route consistently produced larger crystallite sizes than the pre-pH adjustment route across all pH conditions, even at the same pH values.

Table 1 Average crystallite size of as-synthesized TiO_2 nanoparticles with various of pH adjustment sequence

Sample code		Lattice constant (a) in (Å)	Lattice constant (c) in (Å)	Volume of unit cell $(Å)^3$	Strain (ϵ)	Average crystallite size (nm)
TiO_2 commercial (P25)		3.7989	9.5416	137.70	0.003773	22.95
Initial-pH 5		3.8456	9.0115	133.27	0.004655	24.02
Pre-pH adjustment	pH 3	3.7928	9.5184	136.92	0.005184	16.38
	pH 7	3.8064	9.5028	137.68	0.005103	15.62
	pH 10	3.7884	9.5339	136.83	0.005523	17.65
Post-pH adjustment	pH 3	3.7921	9.4994	136.60	0.005227	17.58
	pH 7	3.7983	9.5107	137.21	0.004378	18.50
	pH 10	3.7995	9.5218	137.46	0.004394	19.24

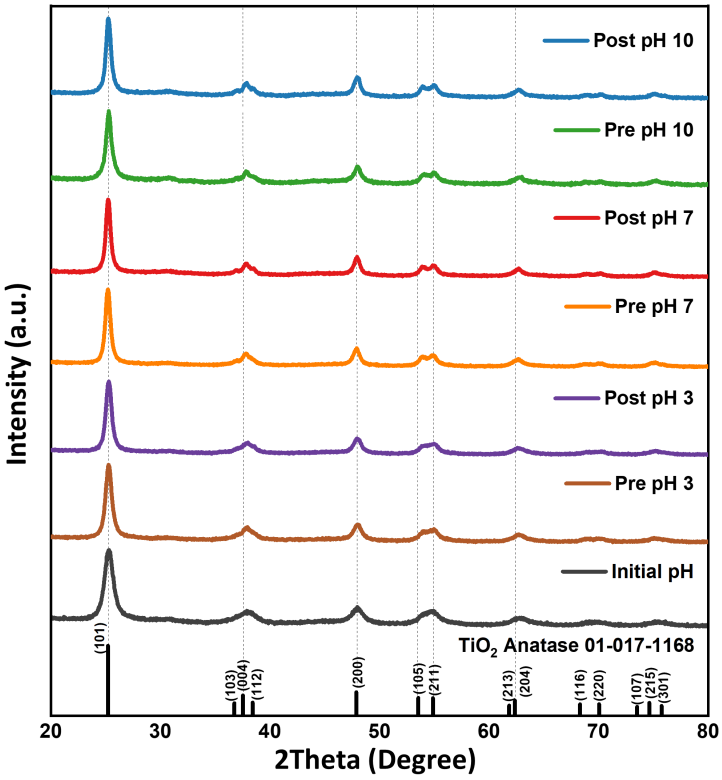

Figure 3 XRD diffraction of as-synthesized TiO_2 nanoparticles with various of pH adjustment sequence

In the pre-pH adjustment route, the pH of the solution is controlled before adding the titanium precursor, which accelerates the hydrolysis of titanium alkoxide. This rapid hydrolysis generates several small nuclei within a short time, leading to the formation of smaller TiO_2 NPs with lower crystallinity. The abundance of hydroxyl ions promotes fast condensation and nucleation, thereby limiting subsequent particle growth (Yalcin, 2022; Sridevi et al., 2020). Hence, during the post-pH adjustment process, hydrolysis proceeds more gradually, resulting in the formation of fewer nuclei. Consequently, crystal growth dominates over nucleation, leading to the production of larger TiO_2 particles.

Moreover, the hydrolysis and condensation kinetics in the sol–gel process are highly dependent on the pH environment. Under acidic conditions (pH $<$ 4), the hydrolysis reaction generally proceeds faster than condensation because the transition states can be more effectively stabilized by the alkoxy (–OR) groups. This favors the formation of short Ti–O–Ti linkages in the early sol–gel stage, which subsequently undergo branching and cross-linking during the aging process. In contrast, under basic conditions, a higher concentration of hydroxyl ions stabilizes the transition intermediates, accelerating both hydrolysis and condensation. Consequently, extensive Ti−O−Ti network formation occurs, leading to the development of larger agglomerates and denser particle assemblies (Imanieh et al., 2010). Therefore, both the timing and pH of adjustment are critical parameters that govern the balance between nucleation and growth, ultimately determining the agglomeration behavior, particle size, and morphology of TiO_2 synthesized via the sol–gel route.

Figure 4(a–f) presents the surface morphology of the as-synthesized TiO_2 nanoparticles obtained under different pH adjustment conditions (initial, pre-pH, and post-pH 10). The FESEM images revealed that the particles exhibited a strong tendency to agglomerate, forming clusters and irregular aggregates with limited dispersion. Such agglomeration behavior is commonly observed in sol–gel–derived TiO_2 systems, where nanoparticles undergo a self-organization process involving nucleation, growth, ripening, and sintering. At higher magnification (Figures 4b, d, and f), smaller particles can be observed on the larger aggregate surfaces. This morphological

feature is consistent with the findings of Chen and Kumar, 2012, who reported that primary particles, which are small, amorphous nanocrystalline units formed during the early sol–gel stage, serve as the fundamental building blocks of TiO_2. These primary particles tend to aggregate and integrate through condensation or partial sintering, forming larger aggregates (secondary particles) that are more compact, and exhibit lower surface area (Chen and Kumar, 2012).

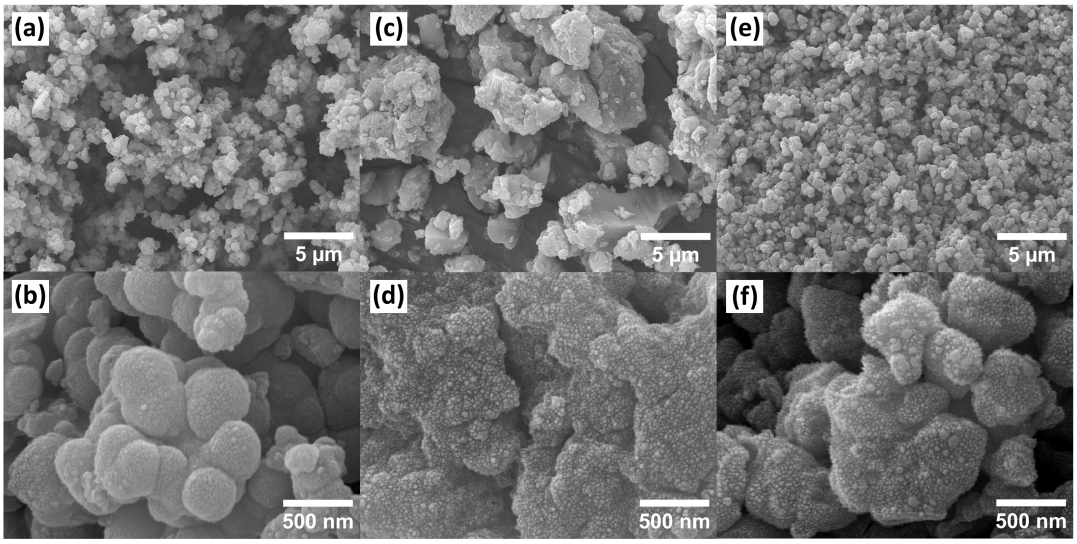

Figure 4 FESEM images of TiO_2 nanoparticles synthesized at different pH adjustment sequences: initial pH 5 (a, b), pre-pH 10 (c, d), and post-pH 10 (e, f), shown at 5.000x× (a, c, e) and 50.000x× (b, d, f) magnifications

Green-synthesized TiO_2 nanoparticles derived from J. multifida leaf extract were evaluated as photoanode materials in DSSCs. The current–voltage (I–V) characteristics, presented in Figure 5, illustrate the relationship between current density and applied voltage. Table 2 summarizes the corresponding photovoltaic parameters. The DSSC fabricated with commercial TiO_2 (P25) achieved a PCE of 3.34%. Notably, the PCEs of the pH 3 samples from both pre- and post-pH adjustment routes surpassed that of the commercial TiO_2 with PCEs of 5.52% and 5.16%, respectively. This improvement indicates that the green synthesis process produces TiO_2 with favorable structural and characteristics, which contribute to enhanced dye adsorption, electron transport, and interfacial charge transfer. These results are consistent with the crystallite size analysis, where the pH 3 sample exhibited a smaller crystallite size. Smaller crystallites generally correspond to higher surface areas, which promote increased dye loading and, consequently, improved DSSC performance (Ashrafuzzaman et al., 2025; Fan et al., 2017).

Furthermore, variations in the timing of pH adjustment significantly influenced the nucleation and growth kinetics of TiO_2 nanoparticles, resulting in distinct particle morphologies, size distributions, and surface areas. The dye adsorption capacity, light-harvesting efficiency, and charge-transport dynamics within the photoanode are determined by these physicochemical properties. Specifically, a high surface area enhances dye uptake, whereas an interconnected particle network facilitates electrolyte diffusion and suppresses charge recombination (Ashrafuzzaman et al., 2025; Karim et al., 2019; Ye et al., 2015).

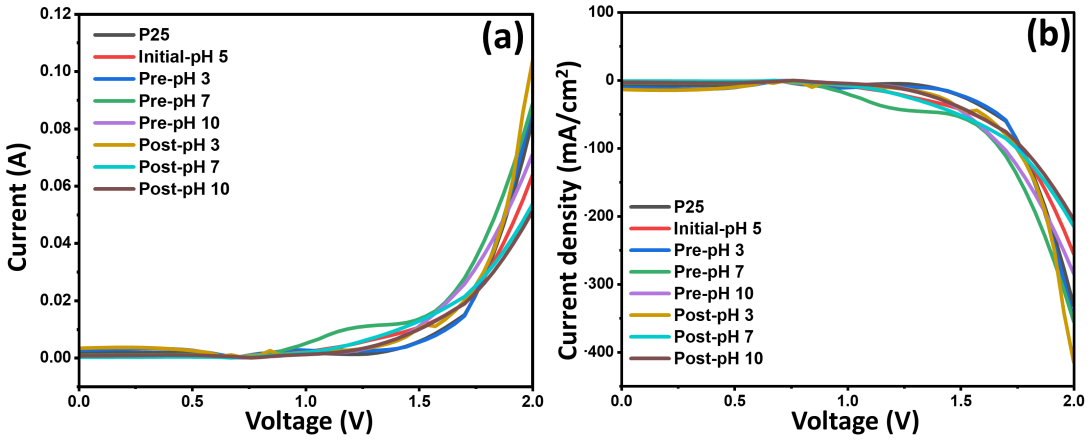

Figure 5 I–V characteristic (a) and current density (b) curve of DSSCs based on as-synthesized TiO_2 nanoparticles with different pH adjustment sequences

Table 2 Comparison of photovoltaic characteristics of DSSCs based on as-synthesized TiO_2 nanoparticles with different pH adjustment sequences

Sample code		Jsc (mA/cm^2)	Voc (V)	FF	PCE (%)
TiO_2 commercial (P25)		6.90	0.71	68.20	3.34
Initial-pH 5		2.82	0.73	81.96	1.69
Pre-pH adjustment	pH 3	10.38	0.70	76.07	5.52
	pH 7	3.44	0.69	88.80	2.10
	pH 10	1.43	0.73	90.29	0.95
Post-pH adjustment	pH 3	13.33	0.73	53.37	5.16
	pH 7	0.81	0.70	104.27	0.59
	pH 10	2.78	0.75	92.69	1.93

4. Conclusions

TiO_2 nanoparticles with an anatase phase were successfully synthesized through a green method using *J. multifida* leaf extract as a natural reducing and stabilizing agent. The timing of pH adjustment during synthesis was found to play a crucial role in determining the nucleation and growth behavior, thereby influencing the final structure and morphology of TiO_2. When the pH was adjusted before precursor addition (pre-pH adjustment), rapid hydrolysis occurred, leading to smaller nanoparticles due to faster nucleation and stronger interaction with biomolecules in the extract. Conversely, adjusting the pH after precursor addition (post-pH adjustment) resulted in slower nucleation, promoting the formation of larger particles through extended growth. Hence, these structural variations significantly affect the performance of TiO_2 when used as a photoanode material in DSSCs. The pre-pH 3 sample delivered the highest PCE of 5.52% owing to its smaller crystallite size, which enhances the surface area, dye adsorption, and charge transport. Thus, the pre-pH adjustment method is preferable for producing TiO_2 for DSSC applications than the post-pH adjustment method, which tends to yield larger particles. Overall, this approach offers a simple, sustainable, and scalable strategy for tailoring TiO_2 properties for enhanced solar energy conversion efficiency.

Acknowledgements

The authors are grateful for the research support provided by the Directorate of Research Funding and Ecosystem Universitas Indonesia through the Q1 International Indexed Publication Research Grant (PUTI Q1) Year 2025-2026 with contract number of PKS-240/UN2.RST/HKP.05.00/2025. The author would also like to extend their gratitude towards the team at Energy Transition Laboratory (ETL) at Interdisciplinary Engineering (IDE), Faculty of Engineering Universitas Indonesia for characterization facilities used in this research.

Author Contributions

Fairuz Septiningrum: Conceptualization, Methodology, Analysis, Investigation, Writing – original draft preparation. Rizka Fahirah: Methodology, Investigation. Muhammad: Methodology, Investigation. Akhmad Herman Yuwono: Conceptualization, Writing – review & editing, Supervision, Project administration, Funding acquisition. Nofrijon Sofyan: Methodology, Investigation, Supervision. Donanta Dhaneswara: Resources, Supervision. Nelson Jap: Methodology. Danang Pamungkas Priambodo: Investigation.

Conflict of Interest

The authors declare no conflicts of interest.

Declaration of AI

The authors acknowledge the use of ChatGPT (developed by OpenAI) for language editing and assistance in improving the structure and grammar of the manuscript. All content was reviewed and verified by the authors to ensure its accuracy and originality.

References

Aftab, S., Khan, N., Amina, M., Liaqat, I., Alkahtani, S., & Mehdi, M. (2025). Advancements in nanomaterials for solar energy harvesting: Challenges, innovations, and future prospects. *Chemical Engineering Journal*. https://doi.org/10.1016/j.cej.2025.164224

Ahmed, S. F., Mofijur, M., Parthasarathy, P., Rahman, S. M. A., Ong, H. C., Alazwari, M., & Ali, M. A. (2022). Green approaches in synthesising nanomaterials for environmental nanobioremediation: Technological advancements, applications, benefits and challenges. *Environmental Research*, *204*. https://doi.org/10.1016/j.envres.2021.111967

Ashrafuzzaman, M., Rahman, M. M., Saidur, R., & Long, B. D. (2025). A review of photoanode materials, challenges, and outlook of dye-sensitized solar cells. *Journal of Power Sources*. https://doi.org/10.1016/j.jpowsour.2025.236636

Behzad, F., Habibi-Yangjeh, A., Vadivel, S., & Dutta, K. (2021). An overview of the plant-mediated green synthesis of noble metal nanoparticles for antibacterial applications. *Journal of Industrial and Engineering Chemistry*, *94*, 92–104. https://doi.org/10.1016/j.jiec.2020.12.005

Chen, H. S., & Kumar, R. V. (2012). Sol-gel tio$_2$ in self-organization process: Growth, ripening and sintering. *RSC Advances*, *2*(6), 2294–2301. https://doi.org/10.1039/c2ra00782g

Dah-Nouvlessounon, D., Adoukonou-Sagbadja, H., Baba-Moussa, F., Sina, H., Ahouansou, R., & Baba-Moussa, L. (2023). Polyphenol analysis via lc-ms-esi and potent antioxidant, anti-inflammatory, and antimicrobial activities of jatropha multifida l. extracts used in benin pharmacopoeia. *Life*, *13*(9). https://doi.org/10.3390/life13091898

Devadiga, D., Selvakumar, M., Hegde, G., & Bhat, D. K. (2021). Dye-sensitized solar cell for indoor applications: A mini-review. *Journal of Electronic Materials*, 3187–3206. https://doi.org/10.1007/s11664-021-08854-3

Fan, K., Yu, J., & Ho, W. (2017). Improving photoanodes to obtain highly efficient dye-sensitized solar cells: A brief review. *Materials Horizons*, *4*(3), 319–344. https://doi.org/10.1039/c6mh00511j

Gnanasangeetha, D., & Suresh, M. (2020). A review on green synthesis of metal and metal oxide nanoparticles. *Nature Environment and Pollution Technology*, *19*(5), 1789–1800. https://doi.org/10.46488/NEPT.2020.v19i05.002

Golthi, V., Harikrishna, K., Natarajan, S., Rao, K., Reddy, M. G., & Madhavi, V. (2024). Green synthesis of cuo nanorods using jatropha podagrica leaf extract for dye degradation and antibacterial applications. *Nanotechnology for Environmental Engineering*, *9*(3), 375–388. https://doi.org/10.1007/s41204-024-00372-x

Goutam, S. P., Saxena, M., Sahu, R., Kushwaha, H. S., & Tiwari, A. (2018). Green synthesis of tio_2 nanoparticles using leaf extract of jatropha curcas l. for photocatalytic degradation of tannery wastewater. *Chemical Engineering Journal*, *336*, 386–396. https://doi.org/10.1016/j.cej.2017.12.029

Hanafy, M. S., El-Sayed, S., Ammar, R., & El-Maghraby, A. (2020). Green synthesis and characterization of tio_2 nanoparticles using aloe vera extract at different ph value. *Scientific Journal of King Faisal University*, *21*(1), 103–110. https://doi.org/10.37575/b/sci/2020

Hassan, Q., Du, M., Liu, Y., Wu, Z., & Li, Q. (2024). The renewable energy role in the global energy transformations. *Renewable Energy Focus*, *48*. https://doi.org/10.1016/j.ref.2024.100545

Imanieh, M. H., Ghoranneviss, M., Farnia, G., Esmaeili, A., & Hantehzadeh, M. R. (2010). Different morphologies of tio_2 nanostructures in acidic and basic sol-gel method. *Nano*, *5*(5), 279–285. https://doi.org/10.1142/S1793292010002189

Kabir, E., Kumar, P., Kumar, S., Adelodun, B., & Kim, K. H. (2018). Solar energy: Potential and future prospects. *Renewable and Sustainable Energy Reviews*, *82*, 894–900. https://doi.org/10.1016/j.rser.2017.09.094

Karim, N. A., Sulaiman, M. Y., Khan, M. M. A., & Akhtaruzzaman, M. (2019). Nanostructured photoanode and counter electrode materials for efficient dye-sensitized solar cells (dsscs). *Solar Energy*, *185*, 165–188. https://doi.org/10.1016/j.solener.2019.04.057

Lee, K. X., Wong, W. S., Ahmad, M. K., & Zaman, S. (2019). Bio-mediated synthesis and characterisation of silver nanocarrier, and its potent anticancer action. *Nanomaterials*, *9*(10), 1–19. https://doi.org/10.3390/nano9101423

Liu, Q., & Wang, J. (2019). Dye-sensitized solar cells based on surficial tio_2 modification. *Solar Energy*, *184*, 454–465. https://doi.org/10.1016/j.solener.2019.04.032

Mohammadian-Sarcheshmeh, H., Arazi, R., & Mazloum-Ardakani, M. (2020). Application of bifunctional photoanode materials in dsscs: A review. *Renewable and Sustainable Energy Reviews*, *134*, 110249. https://doi.org/10.1016/j.rser.2020.110249

Mulay, M. R., Patwardhan, S. V., & Martsinovich, N. (2024). Review of bio-inspired green synthesis of titanium dioxide for photocatalytic applications. *Catalysts*, *14*(11). https://doi.org/10.3390/catal14110742

Muniandy, S. S., Adam, F., Mohamed Saad, M. Z., & Subramaniam, S. (2017). Green synthesis of mesoporous anatase tio_2 nanoparticles and their photocatalytic activities. *RSC Advances*, *7*(76), 48083–48094. https://doi.org/10.1039/c7ra08187a

Nethravathi, P. C., Kumar, M. A., Suresh, D., & Nagabhushana, H. (2021). Tio_2 and ag-tio_2 nanomaterials for enhanced photocatalytic and antioxidant activity: Green synthesis using cucumis melo juice. *Materials Today: Proceedings*, *49*, 841–848. https://doi.org/10.1016/j.matpr.2021.05.670

Priyono, B., Huda, A., Prasetyo, I., & Abdullah, M. (2018). Nanostructure properties and dye-sensitized-solar-cell open-circuit voltage of a tio_2 aerogel and pre-hydrothermally treated xerogels. *International Journal of Technology*, *9*(5), 972–982. https://doi.org/10.14716/ijtech.v9i5.1067

Qamar, O. A., Alhajri, M., Alsaidi, M., & Baig, M. M. A. (2024). Upgrading catalytic properties of green synthesized tio_2 for green fuel production from apricot seeds oil. *Fuel*, *355*, 129516. https://doi.org/10.1016/j.fuel.2023.129516

Saini, R., & Kumar, P. (2023). Green synthesis of tio_2 nanoparticles using tinospora cordifolia plant extract and its potential application for photocatalysis and antibacterial activity. *Inorganic Chemistry Communications*, *156*, 111221. https://doi.org/10.1016/j.inoche.2023.111221

Sangeetha, A., Ambli, A., & Nagabhushana, B. M. (2024). Green and chemical synthesis of tio_2 nanoparticles: An in-depth comparative analysis and photoluminescence study. *Nano-Structures and Nano-Objects*, *40*, 101408. https://doi.org/10.1016/j.nanoso.2024.101408

Sarip, N. A., Aminudin, N. I., & Danial, W. H. (2022). Green synthesis of metal nanoparticles using garcinia extracts: A review. *Environmental Chemistry Letters*, *20*(1), 469–493. https://doi.org/10.1007/s10311-021-01319-3

Sasikumar, R., Shanmugam, R., Venkatesh, M., & Gopinath, K. (2024). Dye-sensitized solar cells: Insights and research divergence towards alternatives. *Renewable and Sustainable Energy Reviews*. https://doi.org/10.1016/j.rser.2024.114549

Saud, P. S., Rahman, M. M., Jilani, A., Shah, S. M., & Kim, H. (2024). Dye-sensitized solar cells: Fundamentals, recent progress, and optoelectrical properties improvement strategies. *Optical Materials*. https://doi.org/10.1016/j.optmat.2024.115242

Sawal, M. H., Rosli, M. I., Khan, M. M. R., & Yusoff, N. H. (2023). A review of recent modification strategies of tio$_2$-based photoanodes for efficient photoelectrochemical water splitting performance. *Electrochimica Acta*, *467*, 143142. https://doi.org/10.1016/j.electacta.2023.143142

Shakeel-Ahmad, M., Pandey, A., & Abd-Rahim, N. (2017). Advancements in the development of tio$_2$ photoanodes and its fabrication methods for dye sensitized solar cell (dssc) applications: A review. *Renewable and Sustainable Energy Reviews*, *77*, 89–108. https://doi.org/10.1016/j.rser.2017.03.129

Singh, S., Kumar, V., Kaushal, A., & Sud, D. (2022). Green synthesis of tio$_2$ nanoparticles using citrus limon juice extract as a bio-capping agent for enhanced performance of dye-sensitized solar cells. *Surfaces and Interfaces*, *28*, 101652. https://doi.org/10.1016/j.surfin.2021.101652

Sofyan, N., Muhammad, Ridhova, A., Angellinnov, F., M'rad, M., Yuwono, A. H., Dhaneswara, D., Priyono, B., & Fergus, J. W. (2025). Jasmine flowers extract mediated green synthesis of tio$_2$ nanoparticles and their photocurrent characteristics for dye-sensitized solar cell application. *Materials for Renewable and Sustainable Energy*, *14*(2). https://doi.org/10.1007/s40243-025-00320-y

Sofyan, N., Ridhova, A., Yuwono, A. H., & Udhiarto, A. (2017). Fabrication of solar cells with tio$_2$ nanoparticles sensitized using natural dye extracted from mangosteen pericarps. *International Journal of Technology*, *8*(7), 1229–1238. https://doi.org/10.14716/ijtech.v8i7.692

Sofyan, N., Rilda, Y., & and, A. (2025). Sustainable synthesis of tio$_2$ nanoparticles from gambier leaf extract for enhanced dssc photocurrent response. *Results in Materials*, *27*, 100752. https://doi.org/10.1016/j.rinma.2025.100752

Sridevi, D. V., RamyaDevi, K. T., Jayakumar, N., & Sundaravadivel, E. (2020). Ph dependent synthesis of tio$_2$ nanoparticles exerts its effect on bacterial growth inhibition and osteoblasts proliferation. *AIP Advances*, *10*(9). https://doi.org/10.1063/5.0020029

Srikar, S., Giri, D., Pal, D., Mishra, P., & Upadhyay, S. (2016). Green synthesis of silver nanoparticles: A review. *Green and Sustainable Chemistry*, *6*, 34–56. https://doi.org/10.4236/gsc.2016.61004

Talebzadeh, S., Queffélec, C., & Knight, D. (2019). Surface modification of plasmonic noble metal–metal oxide core–shell nanoparticles. *Nanoscale Advances*, *1*(12), 4578–4591. https://doi.org/10.1039/c9na00581a

Thammaacheep, P., Suriwong, T., Jannoey, P., Khanitchaidecha, W., Nakaruk, A., & Channei, D. (2024). Bio-synthesis of tio$_2$ photocatalyst: A reduced step approach using leaf extract. *Green Chemistry Letters and Reviews*, *17*(1). https://doi.org/10.1080/17518253.2024.2433607

Tryba, B., Morawski, A., Przepiórski, J., Tsumura, T., & Toyoda, M. (2016). Influence of ph of sol-gel solution on phase composition and photocatalytic activity of tio$_2$ under uv and visible light. *Materials Research Bulletin*, *84*, 152–161. https://doi.org/10.1016/j.materresbull.2016.07.035

Uvarov, V., & Popov, I. (2007). Metrological characterization of x-ray diffraction methods for determination of crystallite size in nano-scale materials. *Materials Characterization*, *58*(10), 883–891. https://doi.org/10.1016/j.matchar.2006.09.002

Virkutyte, J., & Varma, R. (2011). Green synthesis of metal nanoparticles: Biodegradable polymers and enzymes in stabilization and surface functionalization. *Chemical Science*, *2*(5), 837–846. https://doi.org/10.1039/c0sc00338g

Wang, Y., He, Y., Lai, Q., & Fan, M. (2014). Review of the progress in preparing nano tio_2: An important environmental engineering material. *Journal of Environmental Sciences*, *26*(11), 2139–2177. https://doi.org/10.1016/j.jes.2014.09.023

Yalcin, M. (2022). The effect of ph on the physical and structural properties of tio_2 nanoparticles. *Journal of Crystal Growth*, *585*, 126603. https://doi.org/10.1016/j.jcrysgro.2022.126603

Ye, M., Wen, X., Wang, M., Iocozzia, J., Zhang, N., Lin, C., & Lin, Z. (2015). Recent advances in dye-sensitized solar cells: From photoanodes, sensitizers and electrolytes to counter electrodes. *Materials Today*, *18*(3), 155–162. https://doi.org/10.1016/j.mattod.2014.09.001